NANO LETTERS



pubs.acs.org/NanoLett
Letter

# Triple Junction Segregation Dominates the Stability of Nanocrystalline Alloys

Annie K. Barnett, Omar Hussein, Maher Alghalayini, Alejandro Hinojos, James E. Nathaniel, II, Douglas L. Medlin, Khalid Hattar, Brad L. Boyce, and Fadi Abdeljawad*

Cite This: Nano Lett. 2024, 24, 9627−9634
Read Online



**ABSTRACT:** We present large-scale atomistic simulations that reveal triple junction (TJ) segregation in Pt−Au nanocrystalline alloys in agreement with experimental observations. While existing studies suggest grain boundary solute segregation as a route to thermally stabilize nanocrystalline materials with respect to grain coarsening, here we quantitatively show that it is specifically the segregation to TJs that dominates the observed stability of these alloys. Our results reveal that doping the TJs renders them immobile, thereby locking the grain boundary network and hindering its evolution. In dilute alloys, it is shown that grain boundary and TJ segregation are not as effective in mitigating grain coarsening, as the solute content is not sufficient to dope and pin all grain boundaries and TJs. Our work highlights the need to account for TJ segregation effects in order to understand and predict the evolution of nanocrystalline alloys under extreme environments.

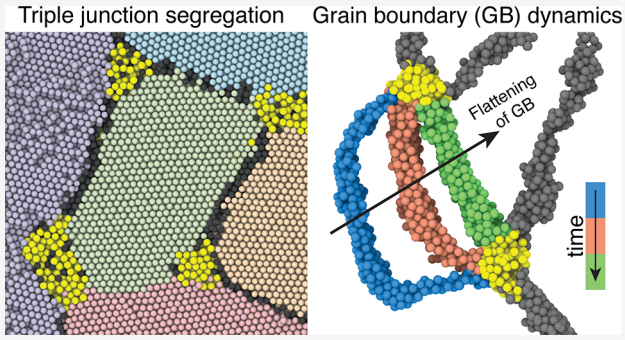


**KEYWORDS:** *triple junction, solute segregation, nanocrystalline materials, atomistic simulations, grain boundary*

Nanocrystalline (NC) materials are characterized by their nanometer-sized crystalline grains that are internally joined through a network of interfaces, termed grain boundaries (GBs), and line defects, termed triple junctions (TJs), where three GBs meet. Owing to their small grain size, NC materials exhibit unique combinations of functionalities including mechanical strength,[1] wear resistance,[2,3] transport properties,[4,5] and electrochemical performance.[6,7] However, the high density of GBs in NC materials renders them thermally unstable with respect to grain coarsening and concomitant evolution of their crystal-size dependent properties even at low homologous temperatures.[8,9] Mitigating grain growth during synthesis and processing treatments or under operating environments remains one of the main hurdles to the use of NC materials in a wide range of engineering applications.[10]

Much of the research dealing with improving the thermal stability of NC metals has been geared toward employing GB solute segregation to mitigate boundary motion.[11,12] With this approach, the NC material is alloyed with an element that preferentially segregates to GBs, which then slows boundary migration and grain growth through various mechanisms.[11−15]

While several studies demonstrated thermally stable NC materials through alloying and subsequent GB segregation,[15−22] absent from such studies is a detailed understanding of the role of TJ solute segregation in the evolution of nanostructures and stability of NC alloys. In addition to GBs, dislocations, and point-defects, TJs are an important part of the repertoire of defects in crystalline solids. Indeed, numerous studies have demonstrated that TJs influence a host of materials phenomena and properties, including diffusion,[23,24] thermoelectric[25] and mechanical[26−28] properties, and GB dynamics.[29−33] To demonstrate the increased contribution of TJs with decreasing grain size, one considers a two-dimensional representation of a NC material with a characteristic grain size $L$ (see Supplementary Figure S-1). For this geometry, the TJ density $\rho_{TJ}$, in units of number of TJs per unit area, and GB density $\rho_{GB}$, in units of length of GB segments per unit area, are related through (see the Supporting Information)

$$\frac{\rho_{TJ}}{\rho_{GB}} \propto \frac{1}{L} \tag{1}$$

Figure 1a is a schematic plot of eq 1 depicting values of $\rho_{TJ}/\rho_{GB}$ for micrometer- and nanometer-size crystalline grains, where a drastic increase in TJ density relative to the GB

Received: May 21, 2024
Revised: July 19, 2024
Accepted: July 19, 2024
Published: July 29, 2024

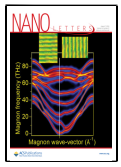

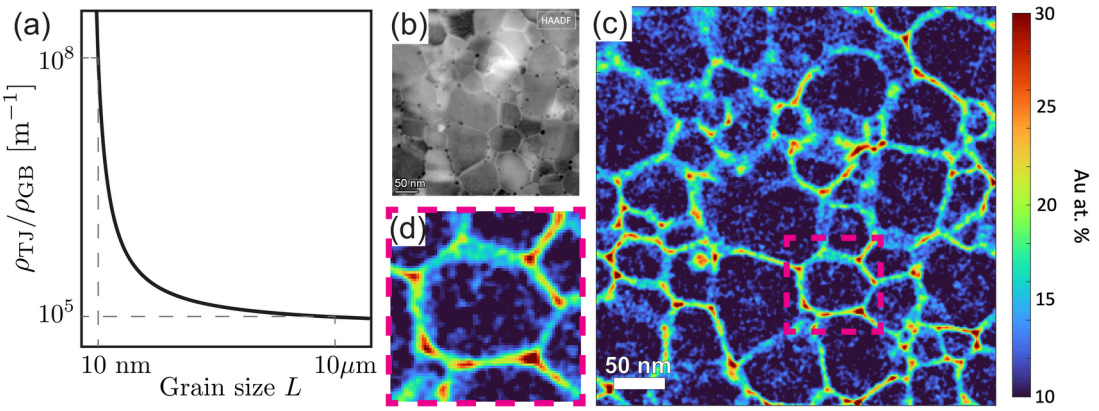


**Figure 1.** (a) Schematic plot of eq 1 showing values of $\rho_{TJ}/\rho_{GB}$ for micrometer- and nanometer-size crystalline grains. For an annealed Pt-10 at. % Au alloy thin film: (b) a representative STEM-HAADF image depicting nanocrystalline grains, (c) quantified Au atomic concentration map of the structure in (b), and (d) an enlargement of the region marked by the dashed line in (c), highlighting increased Au segregation at several TJs. See the Supporting Information for details on sample preparation and data acquisition.

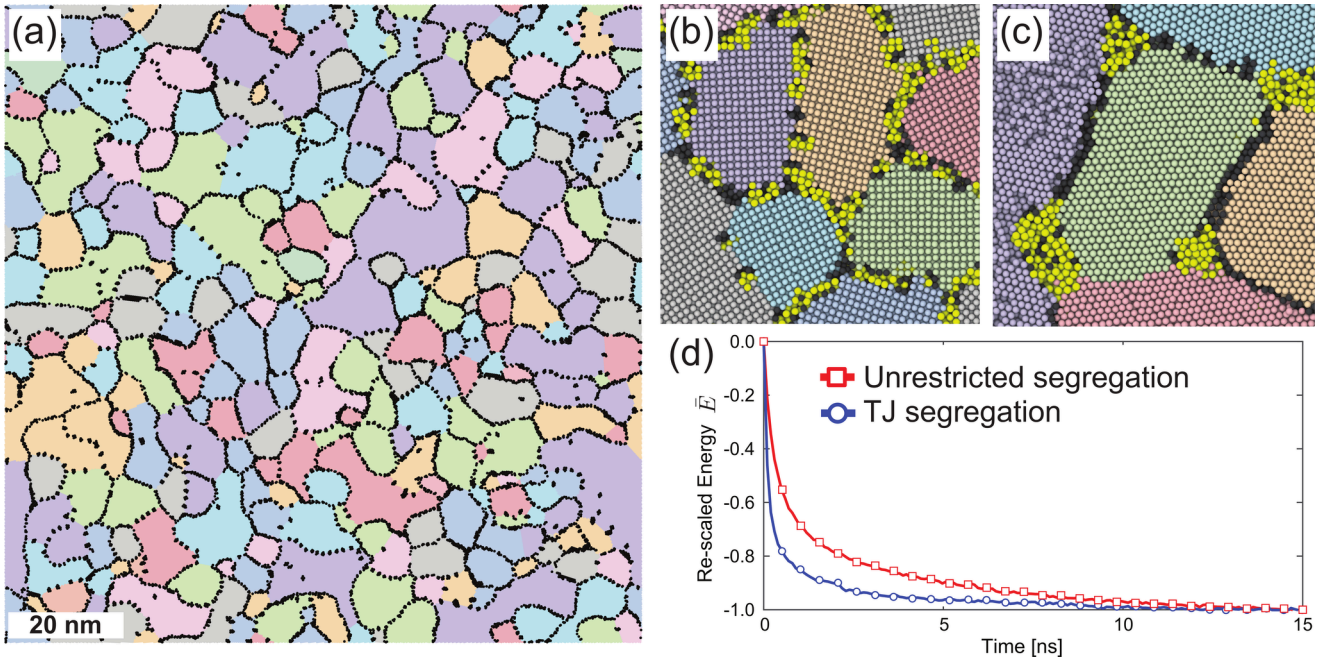


**Figure 2.** (a) Grain structure of a pure NC Pt with a [111] crystallographic direction for the out of plane direction. For a Pt-10 at. % Au alloy, close-up views showing representative (b) unrestricted segregation in [001] and (c) TJ segregation in [111] NC systems. (d) For the [111] NC Pt-10 at. % Au alloy, a plot of the rescaled total energy $\bar{E}(t)$ during MC-MD, where chemical equilibrium is inferred from the asymptotic behavior of $\bar{E}$ curves. In (a–c), nanograins are assigned unique colors, GB atoms are in black, and Au atoms are in yellow.

density is seen as the grain size $L$ is reduced into the nanoscale. Furthermore, since TJs exhibit atomic structures that are distinct from the GBs they are connected to, it is natural for solute atoms to have interactions with TJs that are different than those with GBs.[34−37] Indeed, recent experimental studies revealed solute enrichment at TJs in NC alloys.[22,35,38−40] As a demonstration, Figure 1 shows results for a Pt-10 at. % Au NC alloy, where Figure 1b depicts an image using transmission electron microscopy (TEM) of the nanograin structures in this NC alloy. Figure 1c shows the concentration map, obtained using energy-dispersive X-ray spectroscopy (EDS), of the structure shown in Figure 1b, and Figure 1d is a close-up view of the region marked by the dashed line in Figure 1c, clearly showing strong Au enrichment at TJs in addition to GB segregation. Owing to the geometric degrees of freedom describing GBs and TJs,[41,42] variations in solute segregation levels at these defects can be seen in Figure 1c. The NC Pt−Au alloy thin film was prepared, annealed, and charcterized as discussed in ref 43 (see the Supporting Information). The experimental observations depicted in Figure 1b−d for the NC Pt−Au alloy highlight the need to delineate the role of TJ solute segregation in GB dynamics and grain coarsening in NC alloys.

In this work, we report results of large-scale atomistic modeling studies employing molecular dynamics and Monte Carlo simulations to examine the impact of TJ segregation on the thermal stability of NC alloys. The NC Pt−Au alloy is used as a model system, as Au enrichment to Pt TJs has been experimentally observed here (see Figure 1b−d) and elsewhere.[22,38] Our analysis clearly demonstrates that TJ segregation plays a dominant role in controlling GB dynamics by locking the GB network and limiting its evolution.



https://doi.org/10.1021/acs.nanolett.4c02395
Nano Lett. 2024, 24, 9627−9634

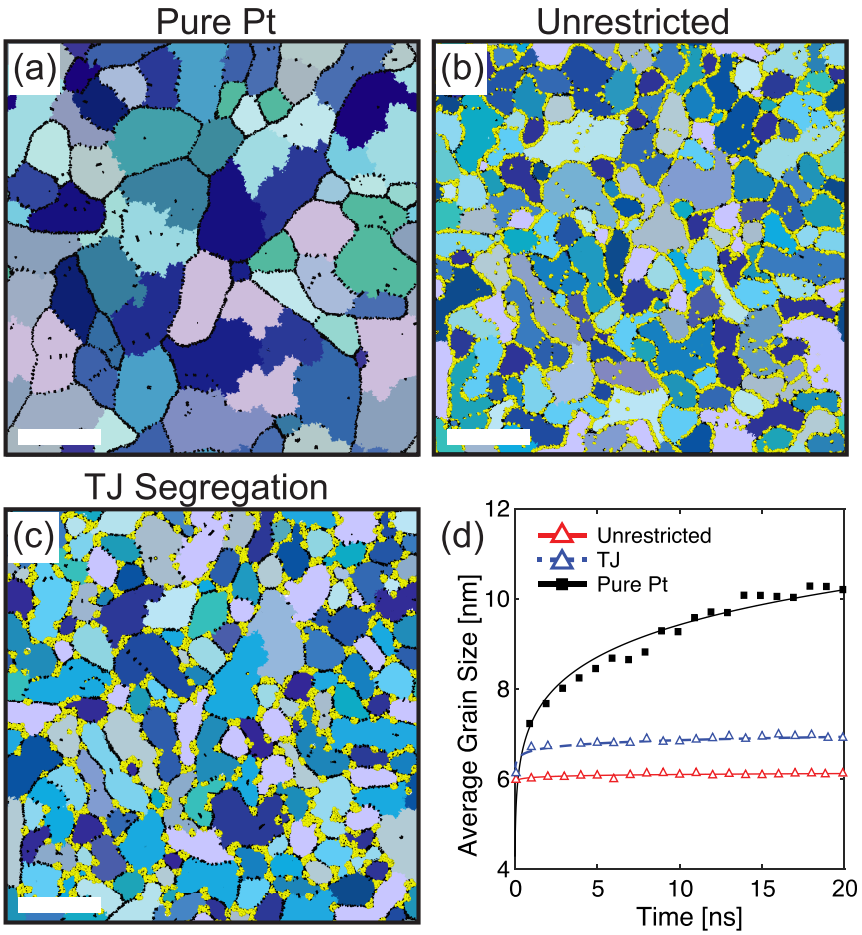


**Figure 3.** Evolution of the grain structures after 20 ns of annealing at 900 K for the (a) pure NC Pt system and (b, c) [111] Pt-10 at. % Au alloys with (b) unrestricted and (c) TJ segregation cases. (d) For the systems depicted in (a−c), temporal evolution of the average grain size. In (a−c), Au atoms are labeled in yellow, nanograins are assigned unique colors, GB atoms are in black, and the scale bars represent 20 nm.

The atomistic simulations are performed using the LAMMPS software package,[44] and visualization of the atomic structures is done using Ovito.[45] We use the interatomic potential by O'Brien et al.,[46] which is fit to capture many of the thermo-physical properties of the Pt−Au alloy across the Au composition space. First, polycrystalline atomistic systems with a wide range of GB types and Au concentrations are generated using the approach outlined in ref 47, which employs grain structures generated from mesoscale models to construct periodic atomistic Pt thin films with columnar grains. Here, the $x$ and $y$ directions define the in-plane coordinates, and the $z$ direction describes the out-of-plane axis. We explore cases with [111] and [001] crystallographic directions for the NC film out-of-plane $z$ axis, where crystalline grains have random in-plane orientations about this common $z$ axis. The overall size of the NC systems is approximately 110 × 110 × 2.4 $nm^3$, resulting in a total number of atoms of approximately 1.25 million atoms. Also, for all systems explored in this work the initial average grain size and total number of grains are ∼5 nm and ∼300, respectively. Figure 2a shows a representative NC Pt system with [111] crystallographic direction for the out-of-plane axis, where the nanograins are assigned unique colors and atoms with non-FCC ordering (i.e., GBs) are labeled in black. In order to examine Au concentration effects, we randomly assign Au atoms to yield NC Pt−Au alloys, where we explore cases with nominal Au concentrations of 1, 5, and 10 at. %.

After the initial construction, the hybrid Monte Carlo (MC)−molecular dynamics (MD) scheme[48,49] is used to equilibrate the atomic structures and compositional degrees of freedom of the NC systems. An MC step is performed with conserved atomic swaps, in which two atoms are randomly selected, and if they are different chemical species, their chemical identities are swapped and accepted with a Boltzmann factor. This MC simulation samples the equilibrium canonical ensemble in a closed system with a fixed number of Pt and Au atoms. In this work, each MC-MD cycle included 500 MC steps followed by a 10 ps MD simulation at 77 K and zero pressure, leading to a trajectory in-phase space that is consistent with the NPT ensemble. This cycle is repeated until the total MC-MD simulation time is 15 ns. In all our MC-MD simulations, a temperature of 77 K is used, as it models cryogenic materials processing routes (e.g., ball milling) commonly used to fabricate NC metallic alloys.[50,51] Once generated and chemically equilibrated using MC-MD, the NC Pt−Au systems are thermally annealed for 20 ns at zero pressure and 900 K, a temperature corresponding to approximately 40% of the solidus temperature for the Pt-10 at. % Au alloy.[52] This high-temperature anneal promotes curvature-driven GB migration where the driving force is related to the boundary's local curvature.[53]

To reveal and quantify the impact of TJ segregation on GB dynamics and the evolution of nanostructures, we consider two solute segregation scenarios for Au. In the first, we allow the


https://doi.org/10.1021/acs.nanolett.4c02395
Nano Lett. 2024, 24, 9627−9634

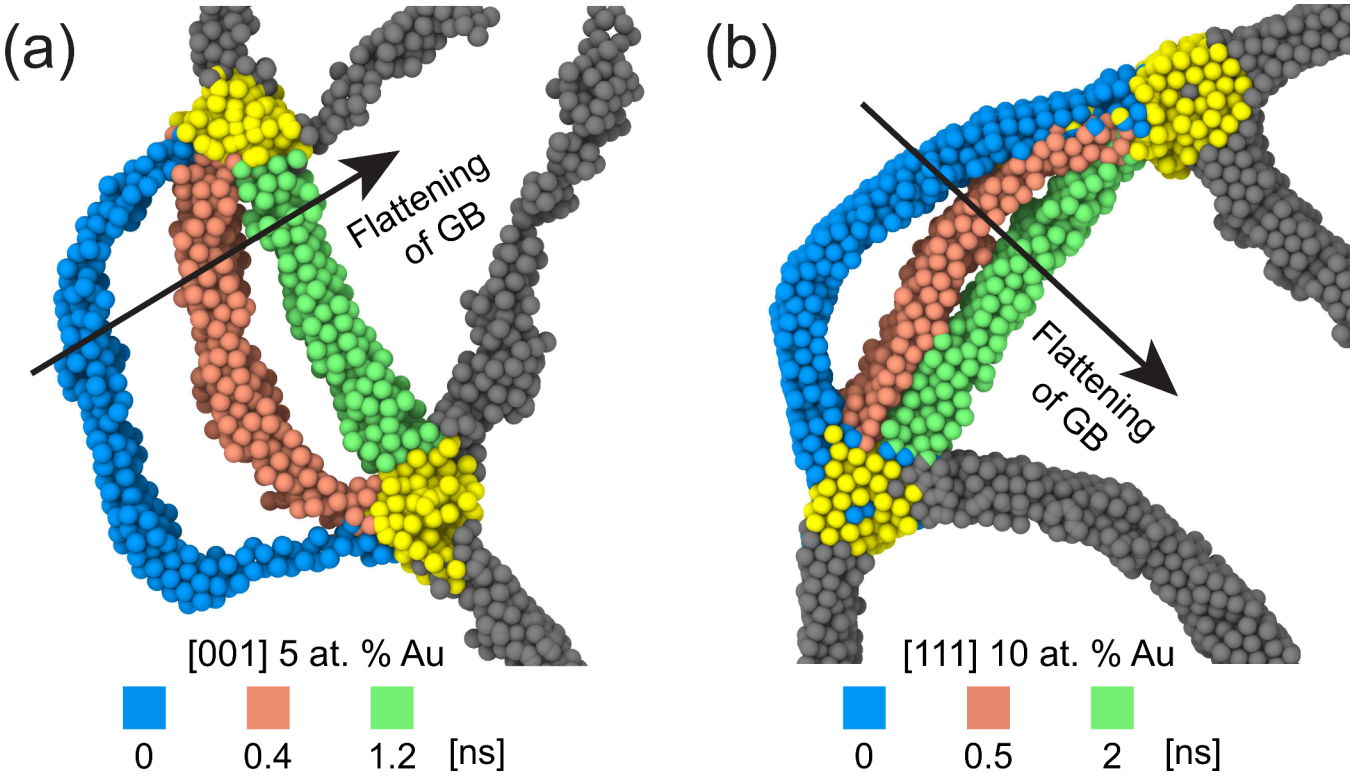


**Figure 4.** Demonstration of how TJ segregation locks the GB network. Snapshots depicting the atomic structure and local GB network near several TJs in (a) [001] Pt-5 at. % Au and (b) [111] Pt-10 at. % Au NC alloys. For a better visualization of the dynamics, the bulk atoms are not displayed and Au atoms are labeled in yellow. The dynamics of one GB are revealed by overlaying boundary atoms at different simulation times and assigning them unique colors. Atoms colored in gray correspond to other GBs connected to the TJs.

MC-MD cycles to take place to any pair of Pt−Au atoms regardless of their position within the NC system. We refer to these cases as *unrestricted* segregation, which mimic solute segregation behavior in experimental NC alloys such as the one depicted in Figure 1b−d. In the second scenario, we only allow Au segregation to TJ regions. This constraint is achieved by defining cylinders of diameter ∼12 Å centered around the TJ lines and restricting the MC-MD swaps to only these TJ regions. We refer to these cases as *TJ segregation*. As a temperature of 77 K is used during the MC-MD stage, the evolution of the TJs is limited during the chemical equilibration step. Again, all our MC-MD studies, including TJ segregation cases, are performed at 77 K and zero pressure. For a Pt-10 at. % Au NC alloy, Figure 2b,c shows respectively close-up views of representative cases of unrestricted Au segregation in a [001] NC alloy and TJ segregation in a [111] NC system, where Au atoms are labeled in yellow, nanograins are assigned unique colors, and GB atoms are depicted in black. To ensure that our MC-MD simulations lead to NC alloys approaching chemical equilibrium, we monitor the rescaled total energy $\bar{E}$ of a NC system given by

$$\bar{E}(t) = \frac{E(t) - E(t=0)}{E(t=0) - E(t=15\ \text{ns})} \tag{2}$$

where a plateau of $\bar{E}$ vs time (i.e., energy is not changing with time) indicates equilibration of the NC alloy chemistry. For example, Figure 2d shows plots of $\bar{E}(t)$ for the [111] NC Pt-10 at. % Au alloy using both unrestricted and TJ segregation cases, where the asymptotic behavior of $\bar{E}(t)$ can be seen indicating chemical equilibrium.

The aforementioned approach of generating and annealing NC Pt−Au systems with [111] and [001] textures and three Au concentrations (i.e., 1, 5, and 10 at. % Au) using unrestricted and TJ segregation cases is intended to be representative of the temperature, Au compositions, and texture observed in recent experimental studies on the thermal stability of NC Pt−Au alloys.[22,38] While we acknowledge that the atomistic systems with unrestricted segregation are more representative of experimentally observed segregation behavior in NC alloys, it is important to emphasize that our computational studies of systems with TJ segregation provide the means to quantitatively describe the relative role of doped TJs in the thermal stability of NC alloys. Also, our computational approach generates crystalline grains with random orientations about the common out-of-plane axis, resulting in GBs and TJs with geometries different from the ones in the experimental NC Pt−Au system in Figure 1. These variations in GB and TJ geometries result in differences in solute segregation levels between our atomistic simulations and the experimental data in Figure 1. Furthermore, while the average grain size in our atomistic simulations is smaller than one in the experimental NC Pt−Au shown in Figure 1b−d, it is important to note that NC materials with an average grain size of less than 10 nm have been synthesized in a wide range of alloys.[54−56]

We begin with comparing the evolution of grain structures in NC systems, specifically pure Pt and Pt−Au alloys with unrestricted and TJ segregation cases. Figure 3a−c shows snapshots of the [111] NC structures after 20 ns of thermal annealing at 900 K, where pure Pt (Figure 3a), Pt-10 at. % Au with unrestricted segregation (Figure 3b), and Pt-10 at. % Au


https://doi.org/10.1021/acs.nanolett.4c02395
Nano Lett. 2024, 24, 9627−9634

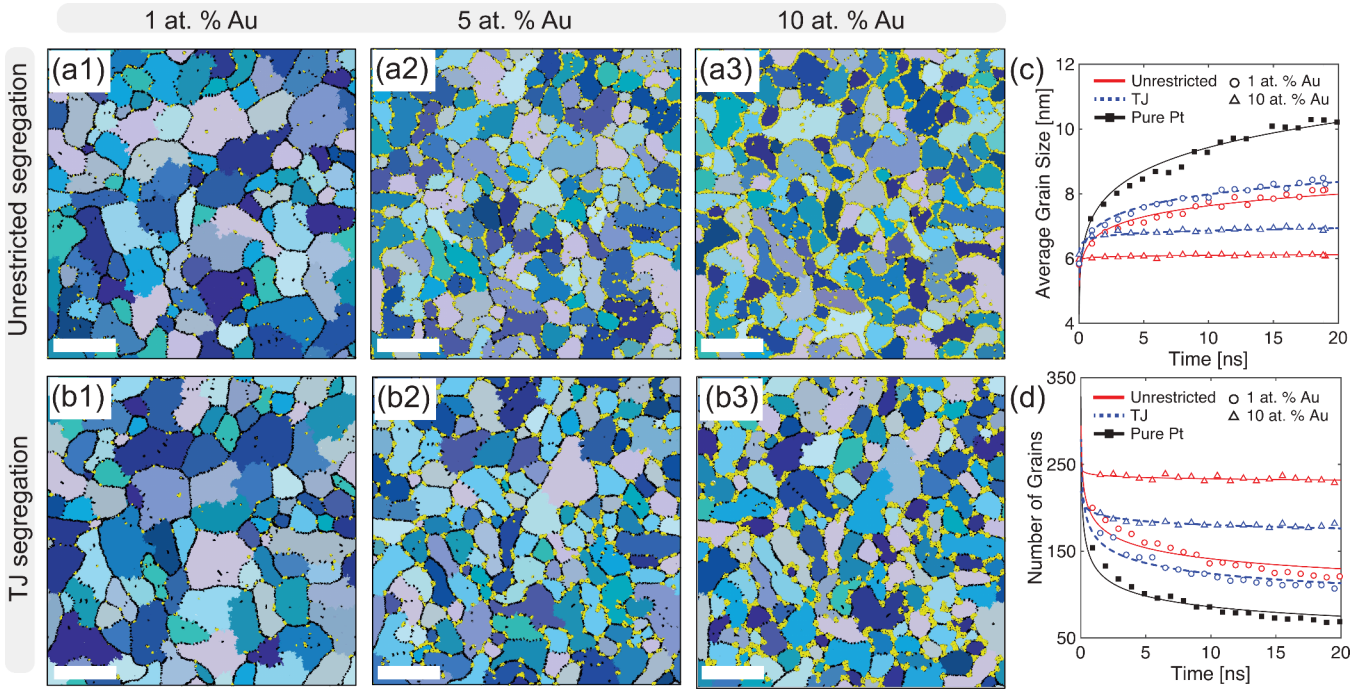


**Figure 5.** For [111] NC Pt−Au films with various Au concentrations, a comparison of the role of TJ segregation in grain coarsening relative to that of unrestricted segregation. Snapshots of the grain structures with (a1−a3) unrestricted and (b1−b3) TJ segregation after annealing at 900 K for 20 ns. Alloys with an Au concentrations of (a1, and b1) 1 at. %, (a2, b2) 5 at. %, and (a3, b3) 10 at. % are shown. Temporal evolution of the (c) average grain size and (d) total number of grains for pure Pt and Pt−Au alloys with 1 and 10 at. % Au. In (a) and (b), Au atoms are labeled in yellow, nanograins are assigned unique colors, GB atoms are depicted in black, and the scale bars represent 20 nm.

with TJ segregation only (Figure 3c) are shown. The initial grain structure for these systems is depicted in Figure 2a. In Figure 3a−c, Au atoms are labeled in yellow, nanograins are assigned unique colors, and GB atoms are depicted in black. NC alloys with unrestricted (Figure 3b) and TJ segregation (Figure 3c) show enhanced thermal stability compared with the pure Pt system (Figure 3a), which experiences rapid grain coarsening. This is shown quantitatively in Figure 3d, which depicts plots of the average grain size as a function of annealing time. The pure Pt system undergoes rapid grain coarsening, where the grains more than doubled in size over 20 ns of annealing at 900 K. This result is in contrast to the cases with TJ and unrestricted segregation, which show a near-flat profile for the average grain size as a function of time. A close examination of Figure 3b,c reveals that the NC alloy with TJ segregation exhibits grain structures that are similar in size to the one with unrestricted segregation. Indeed, Figure 3d shows that after 20 ns of thermal annealing, the average grain size in the NC system with TJ segregation is ∼6.5 nm compared to ∼6 nm in the system with unrestricted segregation and ∼10 nm in pure Pt. The initial average grain size for all NC systems depicted in Figure 3 is ∼5 nm. The results depicted in Figure 3 isolate contributions to thermal stability due to TJ segregation, and it quantitatively demonstrates that doped TJs play an effective role in mitigating grain coarsening in NC alloys.

To reveal how TJ segregation hinders GB migration, we now direct our attention to Figure 4, which depicts representative atomic structures and local GB networks near several TJs for [001] Pt-5 at. % Au (Figure 4a) and [111] Pt-10 at. % Au (Figure 4b) NC alloys. For a better visualization of the structures, the bulk atoms are not displayed and Au atoms in the TJs are labeled in yellow. Furthermore, Figure 4 depicts the dynamics of one GB by overlaying boundary atoms at different simulation times and assigning each unique colors. Atoms colored in gray correspond to other GBs connected to the depicted TJs in Figure 4. It can be clearly seen that Au segregation to TJs renders these line defects immobile, and as a result, the GBs connected to these TJs evolve by flattening their profiles over time, as depicted in Figure 4. Any further migration of these GBs requires the evolution of the TJs to which they are connected, which is hindered due to TJ segregation. This TJ segregation-induced locking of the GB network and flattening of GB profiles shown in Figure 4 has been observed in all atomistic systems employed in this work (see Supplementary Figure S-2 for more examples). While many studies attributed the experimentally observed thermal stability of NC alloys to GB solute segregation and associated mechanisms of energy reduction of the boundary, and thus driving force for grain coarsening[11−13,15] and GB solute drag,[14,57,58] the results depicted in Figures 3 and 4 clearly demonstrate that TJ segregation mitigates grain coarsening in NC alloys by locking the GB network, thereby hindering the migration of GBs.

Finally, we investigate the impact of Au concentration levels on the relative roles of unrestricted and TJ segregation in grain coarsening of NC Pt−Au systems. We employ alloys with Au concentrations of 1, 5, and 10 at. % and consider NC systems with [001] and [111] grain orientations. Figure 5 depicts final structures after 20 ns of thermal annealing at 900 K for [111] NC Pt−Au films with various Au concentrations using both unrestricted and TJ segregation scenarios. Panels in the top row (Figure 5a1−a3) depict unrestricted segregation cases, while panels in the bottom row (Figure 5b1−b3) show systems with TJ segregation only. Pt−Au alloys with an Au concentration of 1 at. % (Figure 5a1,b1), 5 at. % (Figure 5a2,b2), and 10 at. % (Figure 5a3,b3) are shown. In all these


https://doi.org/10.1021/acs.nanolett.4c02395
Nano Lett. 2024, 24, 9627−9634

panels, Au atoms are labeled in yellow, nanograins are assigned unique colors, and GB atoms are depicted in black. Figure 5a,b reveals several trends. First, increasing the Au concentration in NC Pt−Au systems leads to improved stability with respect to grain coarsening. For Pt-10 at. % Au systems, the crystalline grains depicted in Figure 5a3,b3 are considerably smaller in size than those shown in Figure 5a1,b1 for Pt-1 at. % Au. Second, in the small concentration limit shown in Figure 5a1,b1 the Au concentration level is not sufficient to dope and subsequently pin all GBs (Figure 5a1) or TJs (Figure 5b1). Third, a close examination of the non-dilute alloys with unrestricted segregation (Figure 5a2,a3) and the ones with TJ segregation only (Figure 5b2,b3) reveals that TJ segregation plays a dominant role in mitigating grain coarsening and that GB segregation provides a marginal improvement in the thermal stability of NC alloys.

The observations shown in Figure 5a,b are quantified by tracking the temporal evolution of the average grain size (Figure 5c) and total number of grains (Figure 5d) in NC systems with Au concentrations of 1 and 10 at. % (see Supplementary Figures S-3 and S-4 for grain coarsening results for [001] and [111] textures using all Au concentrations). Data for pure NC Pt are shown in Figure 5c,d to provide a baseline for the comparison. Improved thermal stability is observed in both unrestricted and TJ segregation cases, where the increase in average grain size and the decrease in the total number of grains in these systems occur at rates slower than those in pure NC Pt. It is also interesting to note from Figure 5c,d that TJ segregation is as effective in mitigating GB migration and grain coarsening in NC alloys as the cases with unrestricted segregation. For example, after 20 ns of annealing at 900 K, the difference in the average grain size between the system with TJ segregation and the one with unrestricted segregation is ∼0.5 nm for the Pt-10 at. % Au. The quantitative data in Figures 3d and 5c clearly show that TJ segregation plays a major role in mitigating grain coarsening in NC alloys by locking the GB network and that GB segregation (i.e., unrestricted segregation cases) only provides a marginal improvement in the stability of these NC materials.

In summary, we performed large-scale atomistic simulations of solute segregation and high-temperature thermal annealing to examine the impact of TJ segregation on grain coarsening in a model NC Pt−Au alloy. To delineate contributions to the stability of nanostructures due to TJ segregation from those due to GB segregation, we explored two scenarios: unrestricted segregation where Au can segregate anywhere in the NC systems, and TJ segregation, where Au segregation is confined to TJ regions. While simulated systems of unrestricted segregation are more representative of experimentally observed segregation behavior in NC alloys, our computational studies of TJ segregation served to quantitatively describe the relative role of doped TJs in the stability of NC alloys. The NC systems were thermally annealed at 900 K, and the evolution of the grain structures was quantified by tracking the average grain size and number of grains as a function of time. It was shown that Au segregation to TJs renders these line defects immobile, thereby locking the GB network and hindering boundary migration. In dilute alloys, both unrestricted and TJ segregation cases are not as effective in mitigating grain coarsening, as the solute concentration level is not sufficient to dope and pin the GBs or TJs. Our work unequivocally shows that TJ segregation dominates the stability of NC alloys with respect to grain coarsening, and it highlights the need to account for TJ effects in efforts aimed at discovering novel chemistries to fabricate thermally stable NC alloys. Finally, a natural extension of this work would be to explore the interplay among TJ segregation, initial grain size, annealing temperature, and the net impact on the thermal stability of NC alloys.

## ■ ASSOCIATED CONTENT

### Supporting Information

The Supporting Information is available free of charge at https://pubs.acs.org/doi/10.1021/acs.nanolett.4c02395.

Derivation of the triple junction to grain boundary density $\rho_{TJ}/\rho_{GB}$, details on sample preparation and structural and chemical characterization of nanocrystalline Pt−Au alloys, and grain coarsening results for [001] and [111] nanocrystalline Pt−Au alloys using Au concentrations of 1, 5, and 10 at. % (PDF)

## ■ AUTHOR INFORMATION


### Corresponding Author

**Fadi Abdeljawad** − *Department of Materials Science and Engineering, Lehigh University, Bethlehem, Pennsylvania 18015, United States;* orcid.org/0000-0002-4495-4274; Email: fadi@lehigh.edu

### Authors

**Annie K. Barnett** − *Department of Materials Science and Engineering, Johns Hopkins University, Baltimore, Maryland 21218, United States*

**Omar Hussein** − *Department of Physics and Astronomy, George Mason University, Fairfax, Virginia 22030, United States*

**Maher Alghalayini** − *Applied Mathematics and Computational Research Division, Lawrence Berkeley National Laboratory, Berkeley, California 94720, United States*

**Alejandro Hinojos** − *Sandia National Laboratories, Livermore, California 94550, United States*

**James E. Nathaniel, II** − *Sandia National Laboratories, Livermore, California 94550, United States*

**Douglas L. Medlin** − *Sandia National Laboratories, Livermore, California 94550, United States*

**Khalid Hattar** − *Department of Nuclear Engineering, University of Tennessee, Knoxville, Tennessee 37916, United States*

**Brad L. Boyce** − *Center for Integrated Nanotechnologies, Sandia National Laboratories, Albuquerque, New Mexico 87123, United States*

Complete contact information is available at: https://pubs.acs.org/10.1021/acs.nanolett.4c02395


### Notes

The authors declare no competing financial interest.

## ■ ACKNOWLEDGMENTS

F.A. and O.H. acknowledge support from the National Science Foundation (NSF) grant DMR 2114832. A.H., J.E.N., D.L.M., K.H., and B.L.B. received support from the United States (U.S.) Department of Energy (DOE) Office of Basic Energy Sciences (BES), Division of Materials Science and Engineering. Sandia National Laboratories is a multimission laboratory managed and operated by National Technology & Engineering Solutions of Sandia, LLC (NTESS), a wholly owned subsidiary

of Honeywell International Inc., for the U.S. Department of Energy's National Nuclear Security Administration (DOE/NNSA) under contract DE-NA0003525. B.L.B and K.H. performed work at the Center for Integrated Nanotechnologies. This written work is authored by an employee of NTESS. The employee, not NTESS, owns the right, title, and interest in and to the written work and is responsible for its contents. Any subjective views or opinions that might be expressed in the written work do not necessarily represent the views of the U.S. Government. The publisher acknowledges that the U.S. Government retains a nonexclusive, paid-up, irrevocable, worldwide license to publish or reproduce the published form of this written work or allow others to do so, for U.S. Government purposes. The DOE will provide public access to results of federally sponsored research in accordance with the DOE Public Access Plan.

## REFERENCES

(1) Meyers, M. A.; Mishra, A.; Benson, D. J. Mechanical properties of nanocrystalline materials. *Prog. Mater. Sci.* **2006**, *51*, 427−556.
(2) Curry, J. F.; Babuska, T. F.; Furnish, T. A.; Lu, P.; Adams, D. P.; Kustas, A. B.; Nation, B. L.; Dugger, M. T.; Chandross, M.; Clark, B. G.; et al. Achieving ultralow wear with stable nanocrystalline metals. *Adv. Mater.* **2018**, *30*, 1802026.
(3) Wasekar, N. P.; Haridoss, P.; Seshadri, S.; Sundararajan, G. Sliding wear behavior of nanocrystalline nickel coatings: Influence of grain size. *Wear* **2012**, *296*, 536−546.
(4) Chiang, Y.-M.; Lavik, E.; Kosacki, I.; Tuller, H.; Ying, J. Defect and transport properties of nanocrystalline CeO2-x. *Appl. Phys. Lett.* **1996**, *69*, 185−187.
(5) Bueno Villoro, R.; Zavanelli, D.; Jung, C.; Mattlat, D. A.; Hatami Naderloo, R.; Pérez, N.; Nielsch, K.; Snyder, G. J.; Scheu, C.; He, R.; et al. Grain Boundary Phases in NbFeSb Half-Heusler Alloys: A New Avenue to Tune Transport Properties of Thermoelectric Materials. *Adv. Energy Mater.* **2023**, *13*, 2204321.
(6) Soudan, P.; Gaudet, J.; Guay, D.; Bélanger, D.; Schulz, R. Electrochemical properties of ruthenium-based nanocrystalline materials as electrodes for supercapacitors. *Chemistry of materials* **2002**, *14*, 1210−1215.
(7) Wang, S.; Yoon, J.; Kim, G.; Huang, D.; Wang, H.; Jacobson, A. J. Electrochemical properties of nanocrystalline La0. 5Sr0. 5CoO3- x thin films. *Chem. Mater.* **2010**, *22*, 776−782.
(8) Lu, L.; Tao, N.; Wang, L.; Ding, B.; Lu, K. Grain growth and strain release in nanocrystalline copper. *J. Appl. Phys.* **2001**, *89*, 6408−6414.
(9) Andrievski, R. Review of thermal stability of nanomaterials. *J. Mater. Sci.* **2014**, *49*, 1449−1460.
(10) Weertman, J. R. Retaining the nano in nanocrystalline alloys. *Science* **2012**, *337*, 921−922.
(11) Weissmüller, J. Alloy effects in nanostructures. *Nanostructured Materials* **1993**, *3*, 261−272.
(12) Trelewicz, J. R.; Schuh, C. A. Grain boundary segregation and thermodynamically stable binary nanocrystalline alloys. *Phys. Rev. B* **2009**, *79*, 094112.
(13) Chookajorn, T.; Murdoch, H. A.; Schuh, C. A. Design of stable nanocrystalline alloys. *Science* **2012**, *337*, 951−954.
(14) Alkayyali, M.; Abdeljawad, F. Grain boundary solute drag model in regular solution alloys. *Phys. Rev. Lett.* **2021**, *127*, 175503.
(15) Liu, F.; Kirchheim, R. Nano-scale grain growth inhibited by reducing grain boundary energy through solute segregation. *Journal of crystal growth* **2004**, *264*, 385−391.
(16) Chookajorn, T.; Schuh, C. A. Nanoscale segregation behavior and high-temperature stability of nanocrystalline W−20 at.% Ti. *Acta Mater.* **2014**, *73*, 128−138.
(17) Amram, D.; Schuh, C. A. Mechanical alloying produces grain boundary segregation in Fe−Mg powders. *Scripta Materialia* **2020**, *180*, 57−61.
(18) Ahadi, A.; Kalidindi, A. R.; Sakurai, J.; Matsushita, Y.; Tsuchiya, K.; Schuh, C. A. The role of W on the thermal stability of nanocrystalline NiTiWx thin films. *Acta Mater.* **2018**, *142*, 181−192.
(19) Koch, C.; Scattergood, R.; Darling, K.; Semones, J. Stabilization of nanocrystalline grain sizes by solute additions. *J. Mater. Sci.* **2008**, *43*, 7264−7272.
(20) VanLeeuwen, B. K.; Darling, K. A.; Koch, C. C.; Scattergood, R. O.; Butler, B. G. Thermal stability of nanocrystalline Pd81Zr19. *Acta Mater.* **2010**, *58*, 4292−4297.
(21) Cunningham, W. S.; Mascarenhas, S. T.; Riano, J. S.; Wang, W.; Hwang, S.; Hattar, K.; Hodge, A. M.; Trelewicz, J. R. Unraveling thermodynamic and kinetic contributions to the stability of doped nanocrystalline alloys using nanometallic multilayers. *Adv. Mater.* **2022**, *34*, 2200354.
(22) Barr, C. M.; Foiles, S. M.; Alkayyali, M.; Mahmood, Y.; Price, P. M.; Adams, D. P.; Boyce, B. L.; Abdeljawad, F.; Hattar, K. The role of grain boundary character in solute segregation and thermal stability of nanocrystalline Pt−Au. *Nanoscale* **2021**, *13*, 3552−3563.
(23) Chellali, M. R.; Balogh, Z.; Bouchikhaoui, H.; Schlesiger, R.; Stender, P.; Zheng, L.; Schmitz, G. Triple junction transport and the impact of grain boundary width in nanocrystalline Cu. *Nano Lett.* **2012**, *12*, 3448−3454.
(24) Frolov, T.; Mishin, Y. Molecular dynamics modeling of self-diffusion along a triple junction. *Phys. Rev. B* **2009**, *79*, 174110.
(25) Zong, P.-a.; Wang, Z.; Zhang, C.; Liu, Z.; Chen, M.; Li, W.; Han, Q.; Zhang, Q.; Feng, W.; Wan, C. Boosting thermoelectric performance of BayCo4Sb12 by interlinking large-aspect-ratio silver nanowires at the triple junction of grain boundaries. *Materials Today Energy* **2022**, *26*, 101007.
(26) Wu, M.; Zhou, K.; Nazarov, A. Crack nucleation at disclinated triple junctions. *Phys. Rev. B* **2007**, *76*, 134105.
(27) Zhang, Y.; Jiang, S.; Zhu, X.; Sun, D. Orientation dependence of void growth at triple junction of grain boundaries in nanoscale tricrystal nickel film subjected to uniaxial tensile loading. *J. Phys. Chem. Solids* **2016**, *98*, 220−232.
(28) Song, Z.; Artyukhov, V. I.; Yakobson, B. I.; Xu, Z. Pseudo Hall−Petch strength reduction in polycrystalline graphene. *Nano Lett.* **2013**, *13*, 1829−1833.
(29) Srinivasan, S.; Cahn, J. W.; Jónsson, H.; Kalonji, G. Excess energy of grain-boundary trijunctions: an atomistic simulation study. *Acta Mater.* **1999**, *47*, 2821−2829.
(30) Gottstein, G.; Sursaeva, V.; Shvindlerman, L. S. The effect of triple junctions on grain boundary motion and grain microstructure evolution. *Interface Science* **1999**, *7*, 273−283.
(31) Upmanyu, M.; Srolovitz, D. J.; Shvindlerman, L.; Gottstein, G. Triple junction mobility: A molecular dynamics study. *Interface Science* **1999**, *7*, 307−319.
(32) Johnson, A.; Voorhees, P. A phase-field model for grain growth with trijunction drag. *Acta Mater.* **2014**, *67*, 134−144.
(33) Gottstein, G.; King, A.; Shvindlerman, L. The effect of triple-junction drag on grain growth. *Acta Mater.* **2000**, *48*, 397−403.
(34) Stender, P.; Balogh, Z.; Schmitz, G. Triple junction segregation in nanocrystalline multilayers. *Phys. Rev. B* **2011**, *83*, 121407.
(35) Tuchinda, N.; Schuh, C. A. Triple junction solute segregation in Al-based polycrystals. *Physical Review Materials* **2023**, *7*, 023601.
(36) Yin, K.-M.; King, A. H.; Hsieh, T.; Chen, F.-R.; Kai, J.; Chang, L. Segregation of bismuth to triple junctions in copper. *Microscopy and Microanalysis* **1997**, *3*, 417−422.
(37) Zschiesche, H.; Charai, A.; Alfonso, C.; Mangelinck, D. Methods for Gibbs triple junction excess determination: Ti segregation in CoSi 2 thin film. *J. Mater. Sci.* **2020**, *55*, 13177−13192.
(38) Lu, P.; Abdeljawad, F.; Rodriguez, M.; Chandross, M.; Adams, D.; Boyce, B.; Clark, B.; Argibay, N. On the thermal stability and grain boundary segregation in nanocrystalline PtAu alloys. *Materialia* **2019**, *6*, 100298.
(39) Herbig, M.; Raabe, D.; Li, Y.; Choi, P.; Zaefferer, S.; Goto, S. Atomic-scale quantification of grain boundary segregation in nanocrystalline material. *Physical review letters* **2014**, *112*, 126103.


https://doi.org/10.1021/acs.nanolett.4c02395
*Nano Lett.* 2024, 24, 9627−9634

(40) Peng, Z.; Meiners, T.; Lu, Y.; Liebscher, C. H.; Kostka, A.; Raabe, D.; Gault, B. Quantitative analysis of grain boundary diffusion, segregation and precipitation at a sub-nanometer scale. *Acta Mater.* **2022**, *225*, 117522.
(41) Palumbo, G.; Aust, K. A Coincident Axial Direction(CAD) Approach to the Structure of Triple Junctions in Polycrystalline Materials. *Scripta Metallurgica et Materialia* **1990**, *24*, 1771−1776.
(42) Sutton, A. P.; Balluffi, R. W. *Interfaces in Crystalline Materials*; Clarendon Press: 1996.
(43) Monti, J.; Hopkins, E.; Hattar, K.; Abdeljawad, F.; Boyce, B.; Dingreville, R. Stability of immiscible nanocrystalline alloys in compositional and thermal fields. *Acta Mater.* **2022**, *226*, 117620.
(44) Plimpton, S. Fast Parallel Algorithms for Short-Range Molecular Dynamics. *J. Comput. Phys.* **1995**, *117*, 1−19.
(45) Stukowski, A. Visualization and analysis of atomistic simulation data with OVITO−the Open Visualization Tool. *Modell. Simul. Mater. Sci. Eng.* **2010**, *18*, 015012.
(46) O'Brien, C.; Barr, C.; Price, P.; Hattar, K.; Foiles, S. Grain boundary phase transformations in PtAu and relevance to thermal stabilization of bulk nanocrystalline metals. *J. Mater. Sci.* **2018**, *53*, 2911−2927.
(47) Gruber, J.; Lim, H.; Abdeljawad, F.; Foiles, S.; Tucker, G. J. Development of physically based atomistic microstructures: the effect on the mechanical response of polycrystals. *Comput. Mater. Sci.* **2017**, *128*, 29−36.
(48) Foiles, S. Calculation of the surface segregation of Ni-Cu alloys with the use of the embedded-atom method. *Phys. Rev. B* **1985**, *32*, 7685.
(49) Sadigh, B.; Erhart, P.; Stukowski, A.; Caro, A.; Martinez, E.; Zepeda-Ruiz, L. Scalable parallel Monte Carlo algorithm for atomistic simulations of precipitation in alloys. *Phys. Rev. B* **2012**, *85*, 184203.
(50) Zhou, F.; Liao, X.; Zhu, Y.; Dallek, S.; Lavernia, E. Microstructural evolution during recovery and recrystallization of a nanocrystalline Al-Mg alloy prepared by cryogenic ball milling. *Acta Mater.* **2003**, *51*, 2777−2791.
(51) Perrin, A. E.; Schuh, C. A. Stabilized nanocrystalline alloys: The intersection of grain boundary segregation with processing science. *Annu. Rev. Mater. Res.* **2021**, *51*, 241−268.
(52) Okamoto, H.; Massalski, T. The Au- Pt (Gold-Platinum) system. *Bulletin of Alloy Phase Diagrams* **1985**, *6*, 46−56.
(53) Gottstein, G.; Shvindlerman, L. S. *Grain boundary migration in metals: thermodynamics, kinetics, applications*; CRC Press: 2009.
(54) Darling, K. A.; Chan, R. N.; Wong, P. Z.; Semones, J. E.; Scattergood, R. O.; Koch, C. C. Grain-size stabilization in nanocrystalline FeZr alloys. *Scripta Materialia* **2008**, *59*, 530−533.
(55) Rupert, T. J.; Schuh, C. A. Sliding wear of nanocrystalline Ni−W: structural evolution and the apparent breakdown of Archard scaling. *Acta Mater.* **2010**, *58*, 4137−4148.
(56) Roy, A.; Devanathan, R.; Johnson, D. D.; Balasubramanian, G. Grain-size effects on the deformation in nanocrystalline multi-principal element alloy. *Mater. Chem. Phys.* **2022**, *277*, 125546.
(57) Cahn, J. W. The impurity-drag effect in grain boundary motion. *Acta Metall.* **1962**, *10*, 789−798.
(58) Mishin, Y. Solute drag and dynamic phase transformations in moving grain boundaries. *Acta Mater.* **2019**, *179*, 383−395.


https://doi.org/10.1021/acs.nanolett.4c02395
*Nano Lett.* 2024, 24, 9627−9634